We are IntechOpen, the world's leading publisher of Open Access books Built by scientists, for scientists

4,800
Open access books available

122,000
International authors and editors

135M
Downloads

Our authors are among the

154
Countries delivered to

TOP 1%
most cited scientists

12.2%
Contributors from top 500 universities

CLARIVATE ANALYTICS BOOK CITATION INDEX INDEXED

WEB OF SCIENCE™

Selection of our books indexed in the Book Citation Index in Web of Science™ Core Collection (BKCI)

Interested in publishing with us?
Contact book.department@intechopen.com

Numbers displayed above are based on latest data collected.
For more information visit www.intechopen.com

12

Critical State Analysis Using Continuous Reading SQUID Magnetometer

Zdeněk Janu[1], Zdeněk Švindrych[2], Ahmed Youssef[3] and Lucia Baničová[4]
[1,2]*Institute of Physics AS CR, v.v.i., Prague*
[3,4]*Charles University in Prague, Faculty of Mathematics and Physics, Prague*
Czech Republic

1. Introduction

The critical state in type II superconductors determines the maximum current the superconductor can carry without an energy dissipation. The critical state results from a competition between the Lorentz force acting on flux lines (quantized vortices), thermal agitation, pinning force, and repulsive interaction between flux lines. The pinning force localizes the flux lines on crystal lattice defects (dislocations, voids or impurities) and favors glassy state of flux lines, whereas the repulsive interaction between vortices results in a regular flux line lattice. Materials with a strong pinning are called hard superconductors. Such materials are relevant for power application of superconductors: solenoids for high magnetic fields or cables for large transport currents. Recently, high temperature superconductor (HTS) materials with the critical current density j_c of the order of 100 GA m^{-2} at zero temperature and zero applied field were prepared. The second generation of HTS wires (2GHTSC) is constituted from RE-$Ba_2Cu_3O_{6+x}$ (YBCO) films. The critical current density is one or two orders higher than was achieved in $Bi_2Sr_2CaCu_2O_{8+x}$ (BSCCO) round wires or MgB_2, Nb-Ti, Nb_3Sn, and Nb_3Al wires. Unlike BSCCO wires whose performance is lowered by a flux flow at temperature above 35 K the YBCO wires operate even at liquid nitrogen temperature. Another important field of application of superconductors is superconducting electronics. Most of today's superconducting electronics like superconducting quantum interferometer devices (SQUIDs), radiation detectors (SIS mixers), etc. are made of Nb, NbN, or HTS films. The flux lines trapped in the superconducting film may deteriorate sensor sensitivity as the moving flux lines generate noise (Wellstood et al., 1987). The above mentioned elucidates an interest in flux dynamics in thin films, particularly models to a disk and stripe.

The critical state is affected by material properties, the wire or sensor geometry (shape), applied current, field, and temperature. Conventionally the critical state is studied (judged) using contact measurements (four probe resistive method) or magnetic measurements (local magnetization profile or magnetization loops). The latter method eliminates the need for electrical contacts and allows us to study the response of the critical state to an applied magnetic field. Frequency dependent magnetization loops reveal a flux creep or flux flow while nonlinear magnetization loops reveal surface or bulk pinning. In order to analyze these magnetic measurements we need appropriate models. In general, these model represent solution of 3D+t partial differential equations for a magnetic vector potential or flux density.

Numerical methods apply to conductors and superconductors with axial symmetry, but otherwise with an arbitrary cross section like cylinders of finite length, thin and thick disks, cones, spheres, and rotational ellipsoids. The specimen may even be inhomogeneous and anisotropic as long as axial symmetry pertains (Brandt, 1998). Complete analytical solutions are known only for particular geometries and quasistatic behavior of the magnetic flux when the problem may be reduced to 2D. Two such examples are thin disk and strip in Bean critical state in perpendicular magnetic field.

For magnetization loop measurements, one needs a low frequency magnetic field and low frequency sensor of the magnetic moment of the sample. The whole system should be of high linearity, flat frequency and phase dependence - good choice is the superconducting solenoid and SQUID magnetometer. However, commercial SQUID magnetometers are not suitable for such measurements because the solenoid operates in a persistent mode during a measurement and settling time (dead time) affects (slows down) the measurement.[1] Further, a residual field in the high field solenoid causes a nonlinear $H(I)$ dependence. Since the magnetic moment of the sample is measured differentially, reciprocating the sample punctuates the measurement.

2. Continuous reading SQUID magnetometer

An operation of a continuous reading SQUID magnetometer (CRSM) with an immobile sample is based on detection coils in a gradiometer arrangement, which are insensitive to the homogeneous time varying applied magnetic field, but respond to the magnetic sample placed in proximity of one of the coils. A spontaneous or induced magnetic moment of the sample creates a difference in a magnetic flux in the coils and generates a current in an input coil of the SQUID. The SQUID thus measures the variations in the magnetic moment of the sample. Since the sample is immobile no noise or disturbances are generated due to a sample motion and measurement is not interrupted due to a reciprocating sample or sample positioning. The applied field is generated by a superconducting solenoid operating in a nonpersistent mode.

We use SQUID magnetometers in two basic configurations: Standard Sensitivity and High Sensitivity. In a Standard Sensitivity SQUID Magnetometer (SSSM), the superconducting solenoid, gradiometer, and SQUID are immersed in a liquid helium bath, see Fig. 1. The sample holder with a sample temperature sensor is placed inside an anticryostat.

In a High Sensitivity SQUID Magnetometer (HSSM), the superconducting solenoid, gradiometer, SQUID, and a sample holder with a temperature sensor and heater are placed in a copper vacuum chamber with an inset lead can, see Fig. 1. While the solenoid, gradiometer and SQUID are thermally anchored to the vacuum chamber immersed in a cooling liquid helium bath, the sample is mounted on a block suspended on a support with a low thermal conductivity.

2.1 Applied field generation

The applied homogeneous field is generated using a superconducting solenoid operating in the non-persistent mode. The solenoid is wound with a Nb-Ti wire (number of layers) on a coil-former. The solenoid is supplied from a current source driven by a digital to analog converter (DAC) of a data generation/acquisition card.[2] These $\Sigma - \Delta$ DAC

[1] Quantum Design.
[2] National Instruments PC card model PCI-4451.

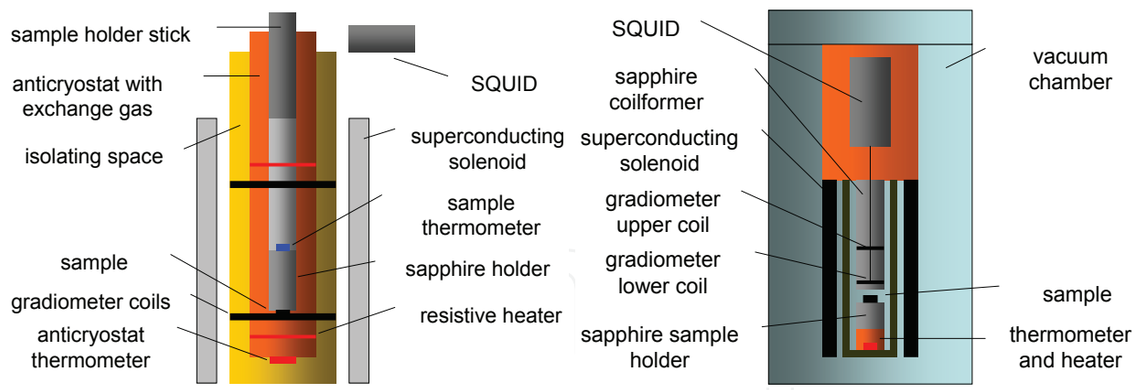

(a) The standard sensitivity magnetometer. (b) The high sensitivity magnetometer.

Fig. 1. Schematic drawing of the SQUID magnetometer

have superior linearity and dynamic range. An applied field $h(t)$ may essentially be of an arbitrary waveform: an AC field superimposed on a DC field for measurement of temperature dependence of susceptibility, with a linear or sinusoidal sweep for measurement of magnetization loops, pulse or step-like for relaxation measurements, frequency sweep, etc. The waveform is designed numerically.

	SSSM	HSSM
Field range (Setting resolution)	$\pm$25 mT ()	$\pm$4 mT ()
Frequency range	DC - 100 Hz	DC - 100 Hz
Temperature range	4.2 - 300 K	4.2 - 150 K
Temperature rate	0.001 - 1 K/min	0.001 - 1 K/min
Sensitivity	7 pA m^2 Hz$^{-1/2}$	5 fA m^2 Hz$^{-1/2}$

Table 1. The parameters of the magnetometers.

Another important property of a SQUID magnetometer is the degree of homogeneity of the applied magnetic field (both in z and r direction). High homogeneity solenoids generating a DC bias field have the homogeneity of the order of 10^{-4} over 4 cm (Vrba, 2001).

2.2 Detection system

The detection system includes superconducting flux transformer and the SQUID. The transformer comprises of coils in a gradiometric arrangement. Two coils with an opposite winding (sense) direction and areas $\mathbf{S}_1$ and $\mathbf{S}_2$ form a first order axial gradiometer which is insensitive to the homogeneous applied field H_0. A balance of the gradiometer, defined as

$$\eta = (\mathbf{S}_1 + \mathbf{S}_2) \cdot \mathbf{S}_1 / |\mathbf{S}_1|^2 \tag{1}$$

is $\eta = 0$ in an ideal case. In practise, any gradiometer is manufactured with a finite mechanical precision and the balance $\eta = 0.0001$ may be achieved with a careful construction (Vrba, 2001).

An inhomogeneous applied field and imperfect gradiometer balance result in a crosstalk of the field to the SQUID and reduce a dynamic range of the CRSM. In SSSM a compensation coil wound on an upper part of the solenoid and supplied with an adjustable current derived from the solenoid supply current minimizes crosstalk. A careful design and construction keeps down deformation of the field affected by a proximity of magnetic or superconducting materials (solder) and frequency dependent eddy currents in metallic (nonsuperconducting) parts.
The magnetic moment of the sample is

$$\mathbf{m} = \frac{1}{2}\int_V (\mathbf{r}\times\mathbf{j})\, d^3r. \tag{2}$$

A vector potential of the induced or spontaneous magnetic moment $\mathbf{m}$ of the sample is

$$\mathbf{A} = \mu\frac{\mathbf{m}\times\mathbf{r}}{r^3}. \tag{3}$$

The magnetic flux in the pickup coil is

$$\Phi = \oint_\Gamma \mathbf{A}\cdot d\mathbf{l}, \tag{4}$$

where Γ is the coil circumference. The SQUID indicates difference in the flux in an upper and lower coil, $\Delta\Phi = \Phi_{upper} - \Phi_{lower}$, and thus the SQUID output voltage is proportional to a projection of the measured magnetic moment on a gradiometer axis, $m(t) \propto \Delta\Phi(t)$.
Since the detection system is superconducting, the output voltage $m(t)$ is proportional to the magnetic moment of the sample and not to a rate of change of the magnetic moment like in case of induction magnetometers (ac susceptometer (ACS) or vibrating sample magnetometer (VSM)).
Both the SSSM and HSSM use bulk Nb SQUID of the Zimmerman type operating at the rf frequency of about 40 MHz. The Josephson junction is a point contact type in the SSSM and thin film bridge in the HSSM. Both SQUIDs have an equivalent input flux noise density of the order of $10^{-4}\ \Phi_0\ \mathrm{Hz}^{-1/2}$ in a white noise region (> 1 Hz) and range $\pm 500\ \Phi_0$ limited by a slew rate $10^4\ \Phi_0/\mathrm{s}$.[3]
A shielding of an external dc and time varying electromagnetic field originating from an earth magnetic field and man-made sources is necessary to utilize the extraordinary sensitivity of the SQUIDs. The shielding is ensured by a soft magnetic materials (the cryostat is placed inside the shielding) and superconducting shielding (Tsoy et al., 2000).

2.3 Sample mounting and temperature reading and control

In SSSM a sample is glued on a bottom surface of a cylindrical sapphire holder using a varnish or grease. A sample temperature sensor, the Si or GaAlAs diode[4], is mounted on the upper surface. The sapphire holder is connected to a (nonmagnetic, nonconducting) polyethylene straw that extends a thin wall stainless tube suspended in an anticryostat. Another Si diode

[3] iMAG 303 SQUID: The equivalent input noise for the standard LTS SQUID system is less than $10^{-5}\ \Phi_0\ \mathrm{Hz}^{-1/2}$, from 1 Hz to 50 kHz in the $\pm 500\ \Phi_0$ range. The response is flat from DC to the 3 dB points, slow slew mode 500 Hz (- 3 dB), normal slew mode 50 kHz (- 3 dB). The input inductance of the LTS SQUID is 1.8×10^{-6} H.
[4] Lake Shore or CryoCon

temperature sensor measures temperature of the anticryostat to facilitate better closed-loop temperature control. Two section resistance wire (constantan) heater is wound around the top and bottom part of the anticryostat to ensure uniform warming. Heat is removed from the sample by a ^{4}He gas at atmospheric pressure.
In HSSM the sample is mounted on the upper surface of the sapphire holder. The holder is embedded in a copper block whose temperature is measured using the Si diode sensor. The block is heated using a resistance wire heater and suspended on a low thermal conductivity fibreglass support which removes heat to liquid ^{4}He bath. The sample is in vacuum.
In both magnetometers, a temperature controller[5] connected to the computer regulates temperature with relative stability of 10 ppm and 1 ppm in SSSM and HSSM, respectively, and controls cooling or warming with rate from 1 mK/min to 10 K/min.

2.4 Measurement modes

The magnetometers are designed for measurements of: i) temperature dependence of a response to fixed AC and DC applied magnetic field (temperature dependence of the susceptibility); ii) response to field sweep at fixed temperature and AC field (magnetization loops and AC susceptibility); iii) relaxation of a DC magnetic moment (after applied field pulse or step) as a function of time or temperature; iv) frequency dependence at a fixed DC field and temperature. Additional measurement modes require only a software change.

2.5 Data acquisition

The dynamic range of the SQUID is extraordinary, the range of $\pm 500\ \Phi_0$ and spectral flux noise density of $10^{-4}\ \Phi_0\ \mathrm{Hz}^{-1/2}$ represent output voltage range ± 10 V and voltage noise density 10 μV Hz$^{-1/2}$, a range of 7 orders (140 dB).[6] The frequency response is flat both in a frequency and phase. In slow slew mode the -3 dB point is 100 Hz. The SQUID output signal $m(t)$ falls into an audio range and thus may be easily digitized in "CD" quality as well as the signal of the applied field $H(t)$, recorded on a hard disk, and digitally processed in real time.[7] Processed data file includes temperature readings.

2.6 AC susceptibility measurement (calculation)

Let the time varying applied AC magnetic field is

$$H(t) = H_{ac}\cos(2\pi f_0 t) = H_{ac}\mathrm{Re}\exp(i2\pi f_0 t), \tag{5}$$

where H_{ac} is the amplitude and f_0 is the frequency of the applied field. The complex AC susceptibility of the sample is

$$\chi_n = \frac{\mathcal{M}(nf_0)}{H_{ac}V}, \tag{6}$$

[5] CryoCon model 34
[6] This applies to rf-SQUIDs. The flux noise density in DC SQUIDs is lower, $10^{-6}\ \Phi_0\ \mathrm{Hz}^{-1/2}$, corresponding voltage noise density 0.1 μV Hz$^{-1/2}$, and dynamic range of 9 orders (180 dB).
[7] We use the National Instruments PC cards model PCI-4451 with $\Sigma - \Delta$ digital to analog and analog to digital converters for a digital signal generation and acquisition (two input channels with 16 bit resolution, frequency range from 0 (true DC) to 95 kHz, and sampling rate up to 204.8 kS/s).

where n denotes harmonics and $\mathcal{M}(nf_0)$ are the Fourier components of the magnetic moment $m(t)$. Higher harmonics of the complex susceptibility appear in the case of a nonlinear response to the applied field. Usually the susceptibility is normalized to a volume V (or mass) of the sample. Using the susceptibility, the magnetization loops are

$$M\left(H\left(t\right)\right) = \sum_{n} \chi_n H_{ac} \exp\left(ni2\pi f_0 t\right), \tag{7}$$

A common way to measure the AC susceptibility is to detect a signal of the magnetic moment using a phase sensitive lock-in amplifier, preferably a two phase instrument indicating both real and imaginary part of the AC susceptibility, and drive the AC field using a signal generator. The conventional analog lock-in amplifier multiplies the input signal $m(t)$ by a square wave $r(t)$ derived from a reference signal $H(t)$ and integrates the product. The DC output are in-phase and out-of-phase components

$$\mathrm{Re}\mathcal{M}(f_0) = \frac{4}{\pi\tau}\int_{t-\tau}^{t}\left[\sum_{n=1}^{\infty}\frac{1}{n}\sin(n\frac{\pi}{2})\cos\left(n2\pi f_0 t'\right)\right]m(t')dt', \tag{8}$$

$$\mathrm{Im}\mathcal{M}(f_0) = \frac{4}{\pi\tau}\int_{t-\tau}^{t}\left[\sum_{n=1}^{\infty}\frac{1}{n}\sin\left(n2\pi f_0 t'\right)\right]m(t')dt', \tag{9}$$

where n is odd and τ is the averaging time constant. Since the reference signal $r(t)$ is a square wave, the DC output is proportional not only to the Fourier component of the first harmonic but also to $1/3$ of third, $1/5$ of fifth, etc. Evidently, this way of signal processing is not suitable for the measurement of a nonlinear response. One can apply input filters that sufficiently suppress third and higher odd harmonics, but remain unaffected the fundamental frequency. However, suitable tunable filters are complex and expensive.

In the digital signal processor (DSP) lock-in amplifiers the signal is filtered with a simple anti-aliasing filter and digitized by over-sampling ADC with subsequent digital filtering. The DSP chip then synthesizes digital reference sine (and cosine) wave at the reference frequency nf_0 and multiplies the signal by this reference. After multiplication, stages of digital low-pass filtering are applied to average over the signal period. The DSP lock-in amplifier generates the true rms values of the complex Fourier components of $\mathcal{M}(f_0)$ or nth harmonic $\mathcal{M}(nf_0)$:

$$\mathcal{M}\left(nf_0\right) = \frac{1}{N\Delta t}\sum_{k=0}^{N-1} m\left(t_k\right)\exp\left(ni2\pi f_0 t_k\right), \tag{10}$$

where $\Delta t = t_k - t_{k-1}$ is the sampling interval and $N\Delta t$ is averaging time. However, commercial DSP lock-in amplifiers provide only components at single frequency. Hence, unless successive measurements of the harmonics are done, one needs an extra instrument for the each additional harmonic.

With computational power of today's processors in personal computers (PC) and data generation/acquisition hardware the problem as a whole may be solved much more effectively. The single PC card, with essentially the same ADC as are used in the DSP lock-in amplifier, substitutes for the generator and lock-in amplifiers. Since the DACs generating the applied field and ADCs sampling $m(t)$ and $H(t)$ use the same clock, synchronization is guaranteed. In reality, an approach using a direct digital signal generation, acquisition, and processing is more cost effective and less time consuming.

The nth harmonic of the AC susceptibility is given by generalized Eq. 6,

$$\chi_n = \frac{\mathcal{M}(nf_0)}{H_{ac}\exp(ni\varphi)}, \tag{11}$$

where complex $H_{ac}\exp(ni\varphi) \equiv |\mathcal{H}(f_0)|\exp(ni\arg\mathcal{H}(f_0))$ takes into account a phase of the Fourier component of the applied field $\mathcal{H}(f_0)$, i.e. a time shift between a Fourier transformed data segment and cosine field. The $\mathcal{M}(f)$ and $\mathcal{H}(f)$ spectra are computed using a discrete fast Fourier transform (FFT) of real data arrays $m(t_k)$ and $H(t_k)$.

$$\mathcal{M}_l \equiv \sum_{k=0}^{N-1} m(t_k)\exp\left(i2\pi kl/N\right), \tag{12}$$

(the same holds for $H(t) \Leftrightarrow \mathcal{H}(f)$), where N is the transform length (Press et al., 1992). Spectra of the complex amplitudes $\mathcal{M}(f)$ and $\mathcal{H}(f)$ are calculated for frequencies $l\Delta f$, $\mathcal{M}_l \equiv \mathcal{M}(l\Delta f)$. With an applied FFT algorithm N must be a power of 2, FFT is computed in $N\log N$ operations, and $\Delta f = f_s/N$, where $f_s = 1/\Delta t$ is the sampling frequency.[8] Unlike the DSP lock-in amplifiers, where another instrument performing N operations to process $N\Delta t$ long record is need for each measured harmonic, here the whole frequency spectrum from DC to $f/2$ is computed with only $N\log N$ operations using the single instrument. Computation time takes few ms.

Strictly speaking, the measurement of temperature dependence of the susceptibility represents a continuous measurement of magnetization loops at slowly varying temperature. Since the input signals are recorded as well as temperature readings, various time domain and frequency domain filters may be applied thereupon. The magnetization loops may be processed using different time windows (for example to remove a linear trend in $m(t)$) or different averaging times.

3. Critical state in type II superconductors

3.1 Vortex matter

Type II superconductors, ie. those with $\lambda/\xi > 2^{-1/2}$, where λ is the flux penetration length and ξ is the coherence length of a superconducting order parameter, remain superconducting even in a high magnetic field due to lowering of their energy by creating walls between normal and superconducting regions. Consequently, flux lines (vortices) with a normal core of a radius of $\approx \xi$, where the order parameter vanishes, and persistent current circulating around the core and decaying away from the vortex core at distances comparable with λ are created at sample edges and penetrate into an interior of the superconductor. The vortex is a linear (in three dimensions) object which is characterized by a quantized circulation of the phase of the order parameter around its axis and carries a single quantum of the magnetic flux $\Phi_0 = h/2e$. The superconductor penetrated with the flux lines is called to be in a mixed state. A repulsive interaction between the flux lines eventually forms flux line bundles and consecutively a flux

[8] Let us take $N = 2^{14}$ (16 K samples), easy for real time processing on a common PC. With $f_s = 6.4$ kS/s the $\Delta f = 0.390625$ Hz. A right choice for the AC field frequency f_0 is an integer multiple of Δf. For example, with $f_0 = 4\Delta f = 1.5625$ Hz, one period of the AC field is represented by 4 K samples. In this case the 16 K FFT means averaging over 4 periods (2.56 s) of the AC field. If the 16 K data are shifted by 4 K and a void part is replaced with samples of the latest read period, the spectra are averaged over 2.56 s and updated in 0.64 s interval. The index of the nth harmonics amplitude is $l = n4$.

line lattice. In increasing applied field the flux lines enter into the superconductor when the magnetic field exceeds the lower critical field $H_{c1} \approx \Phi_0/\mu_0\lambda^2$. Type II superconductors experience a second-order phase transition into a normal state at the upper critical field $H_{c2} \approx \Phi_0/\mu_0\xi^2$. In type I superconductors this transition is a first-order in a nonzero field.

3.2 Pinning and surface barrier

In a real type II superconductor there are always crystal lattice distortions, voids, interstitials, and impurities with reduced superconducting properties. The superconducting order parameter is either reduced or suppressed completely, just as within a vortex core. That implies that such defects are energetically favorable places for vortices to reside and the vortices will be pinned in the potential of these so-called pinning centers. The efficiency of such a pinning center is at its maximum if its size is of the order of the coherence length ξ. If there is almost no pinning, flux flow occurs (Bardeen, 1965). On the other hand, when there is finite pinning, flux creep of a vortex bundles takes place (Anderson, 1962; 1964). The bundle size is determined by the competition between pinning and the elastic properties of the vortex lattice.

An edge or surface barrier may oppose a flux entry into the sample (Beek et al., 1996). A surface barrier arises as a result of the repulsive force between vortices and the surface shielding current. The first example is Bean-Livingston barrier, which is a feature of flat type II superconductor surfaces in general and is related to a deformation of the vortex at the surface (mirror vortex). The second example is the edge-shape barrier, which is a geometric effect related to the distribution of the Meissner shielding current density in non-ellipsoidal samples.

When an increasing magnetic field is initially applied, flux cannot overcome the barrier, and $M = -H$. At the field of the first flux penetration H_p, the magnetic pressure is sufficiently high to overcome the barrier. If there is no pinning, vortices will now distribute themselves through the sample in such a way that the bulk current is zero and vortex density is homogeneous.

3.3 Flux line dynamics

When the superconductor is carrying a bulk transport or shielding current density $\mathbf{j}$ the flux lines experience a volume density of the driving Lorentz force $\mathbf{f}_L = \mathbf{j} \times \mathbf{B}$, where $\mathbf{B}$ is the flux density inside the flux line. When the Lorentz force acting on the flux lines is exactly balanced by the pinning force density, i.e. $F_L = F_p$, the current density is called the depinning current density, j_c. Under this force the flux lines may move through the crystal lattice and dissipate energy. In this case the electrical losses are no longer zero. In an ideal (homogeneous) type II superconductor there is nothing to hinder the motion of flux lines and the flux lines distribution is homogeneous. The flux lines can move freely, which is equivalent to a vanishing critical depinning current density j_c. On the other hand, the non-dissipative macroscopic currents are the result of the spatial gradients in the density of flux lines or due to their curvature. This is possible only due to the existence of pinning centers, which can compensate the Lorentz force.

The moving flux lines dissipate energy by two effects which give approximately equal contributions: (a) eddy currents that surround each moving flux line and have to pass through the vortex core, which in the model of Bardeen and Stephen is approximated by a normal conducting cylinder (normal currents flowing through the vortex core) (Bardeen, 1962); (b)

Tinkham's mechanism of a retarded recovery of the order parameter at places where the vortex core has passed (Tinkham, 1996).
In general, the current density in type II superconductors can have three different origins: (a) Surface currents within the penetration depth λ. In the Meissner state the current passing through a thick superconductor is restricted to a thin surface layer where the magnetic field can penetrate. Otherwise the magnetic field due to the current would exist inside the superconductor; (b) A gradient of the flux-line density; (c) A curvature of the flux lines.
A flux line motion is discouraged (inhibited) by pinning of individual flux lines, their bundles or lattice. In cases of flux flow and flux creep, the vortices are considered to move in an elastic bundle. With discovery of HTS, however, more complex forms of vortex motion are considered. When the driving force is small, the vortices move in a plastic manner - plastic flow where there are channels in which vortices move with a finite velocity, whereas in other channels the vortices remain pinned (Jensen, 1988). Thus, between moving channels and static channels there are dislocations in the flux lattice. With further increasing driving current, vortices tend to re-order. Through dynamic melting, a stationary flux lattice changes into a moving flux lattice via the plastic flow (Koshelev & Vinokur, 1994).
If pinning is efficient the critical depinning current density j_c becomes high and the material is interesting for applications. The properties of the flux line lattice and the pinning properties are important for applications; on the other hand they are complex and interesting topics of condensed-matter physics and materials science.

3.4 Equation of motion of vector potential

In general, computation of magnetization loops represents a full treatment of a nonlinear 3D problem described by a partial differential equation for a vector potential

$$\frac{\partial \mathbf{A}}{\partial t} = D\nabla^2\mathbf{A}, \tag{13}$$

where D is the diffusivity. Due to an axial symmetry or for a long sample in a parallel field, the problem may reduce to 2D and the current density $\mathbf{j}$, vector potential $\mathbf{A}$, and electric field $\mathbf{E}$ are parallel to each other and have only a y or ϕ component (applied field is parallel to z axis) (Brandt, 1998). The magnetization loops are obtained solving Eq. 13 using specialized software packages or directly by the time integration of the nonlocal and nonlinear diffusion equation of motion for the azimuthal current density. A long cylinder or slab in parallel field or thin circular disk and strip in an axial field are 1D problems. The flux density and electric field are $\mathbf{B} = \nabla \times \mathbf{A}$ and $\mathbf{E} = -\partial\mathbf{A}/\partial t$, respectively.
In the normal (nonsuperconducting) state with an ohmic conductivity σ is $D = 1/\mu_0\sigma = m/\mu_0 ne^2\tau$. In Meissner state the diffusivity is the pure imaginary $D = i\omega m/\mu_0 n_s e^2$ with a linear frequency dependence, where n_s is the superconducting condensate density.
In an inhomogeneous type II superconductor with flux pinning the electric field is given by nonlinear local and isotropic resistivity $\rho(\mathbf{j})$. A material law $\mathbf{E}(\mathbf{j})$ reflects a flux line pinning. In case of a strong pinning $\mathbf{E}(\mathbf{j})$ is zero up to the critical depinning density j_c at which electric field raises sharply. A power law voltage current relation

$$\mathbf{E}(j) = E_c|j/j_c|^n\mathbf{j}/j = \rho_c|j/j_c|^{n-1}\mathbf{j}, \tag{14}$$

where $j = |\mathbf{j}|$, is observed in numerous experiments (Brandt, 1996). From the theories on (collective) creep, flux penetration, vortex glass picture, and AC susceptibility one obtains the useful general interpolation formula

$$U(J) = U_0 \frac{(j_c/j)^{\alpha} - 1}{\alpha}. \tag{15}$$

Here $U(j)$ is a current-dependent activation energy for depinning which vanishes at the critical current density j_c, and α is a small positive exponent. In the limit $\alpha \to 0$ one has a logarithmic dependence of the activation energy $U(j) = U_0 \ln(j_c/j)$, which inserted into an Arrhenius law yields

$$\mathbf{E}(j) = E_c \exp\left(-\frac{U(j)}{k_B T}\right) = E_c \left(\frac{j}{j_c}\right)^{U_0/k_B T}. \tag{16}$$

When we compare Eq. 16 with Eq. 14 the exponent is $n = U_0/k_B T$. For $\alpha = -1$ the Eq. 15 coincides with the result of the Kim-Anderson model, $E(j) = E_c \exp[(U_0/k_B T)(1 - j/j_c)]$, (Blatter et al., 1994). For $\alpha = 1$ one gets $E(j) = E_c \exp[(U_0/k_B T)(j_c/j - 1)]$.
In general, the E_c and activation energy U in Eq. 16 depend on the local induction $\mathbf{B}(\mathbf{r})$ and thus also $\alpha(\mathbf{B}, T)$ and $j_c(\mathbf{B}, T)$ depend on $\mathbf{B}$.
With $\mathbf{E} = -\partial\mathbf{A}/\partial t$ and Eq. 14 one obtains for the diffusivity in Eq. 13

$$D(j, j_c, U_0, T) = \frac{1}{\mu_0}\frac{\partial \mathbf{E}}{\partial \mathbf{j}} = \frac{1}{\mu_0}\frac{E_c}{j_c}\left(\frac{j}{j_c}\right)^{U_0/k_B T - 1} = \frac{\rho_c}{\mu_0}\left(\frac{j}{j_c}\right)^{U_0/k_B T - 1}. \tag{17}$$

Power-law electric field versus current density (Eq. 14) induces:
i) An Ohmic conductor behavior with a constant resistivity $\rho = E/j$ for $U_0/k_B T = 1$. This applies also to superconductors in the regime of a linear flux flow or thermally activated flux flow (TAFF) at low frequencies with flux-flow resistivity $\rho_f = \rho_n B/\mu_0 H_{c2}$, known as the Bardeen-Stephen model. The diffusivity D is large and vector potential profiles are time dependent. The magnetization loops have a strong frequency dependence, as well as the susceptibility, and the AC susceptibility has only fundamental component independent on the AC field amplitude (Gömöry, 1997).
ii) Flux creep behavior for $1 \ll U_0/k_B T < \infty$. The magnetization loops have a weak frequency dependence, as well as the AC susceptibility which has higher harmonics and is dependent on the AC field amplitude.
iii) Hard superconductors with strong pinning for $U_0/k_B T \to \infty$. In this case the flux dynamics is quasistatic, described by a Bean model of the critical state with $D = 0$ for $|j| < j_c$ and $D \to \infty$ for $|j| = j_c$. The magnetization loops are frequency independent, as well as the AC susceptibility which has higher harmonics and strongly depends on the AC field amplitude.
A general solution of Eq. 13 represents time dependent vector potential profiles which dynamics covers a viscous flow, diffusion (creep), and quasistatic (sand pile like) behavior.
The resistivity generated by the flux creep is Ohmic in the low-driving force limit.

3.5 Analytically solvable models

3.5.1 Normal state with ohmic conductivity and flux flow state

In normal state with an ohmic conductivity $\sigma = ne^2\tau/m$ the diffusion constant is $D = 1/\mu_0\sigma = \omega\delta^2$, where ω is the angular frequency of the applied AC field and $\delta = (2\mu_0\omega\sigma)^{-1/2}$

is the normal skin depth. In this case the analytical solutions to Eq. 13 are known for an infinitely long cylinder and slab in a parallel field, cylinder in a perpendicular field, and sphere (Brandt, 1998; Khoder & Couach, 1991; Lifshitz et al., 1984).
With an increasing ratio δ/R or δ/d, where and R is the radius of the cylinder or sphere and $2d$ id the slab thickness, a sample changes from a diamagnetic (but lossy) at $\delta \ll R$, to absorptive at $\delta \approx R$, and to transparent for applied field at $\delta \gg R$. The magnetization loops $M(H)$ are ellipses which major axis lies on H axis of $H - M$ diagram for transparent medium and gradually turns to $-\pi/4$ direction for diamagnetic medium. The susceptibility as a function of $(\delta/R)^2$ is shown in Fig. 2.
In a limit of low frequencies when the skin depth $\delta \gg R, d$ and the sample is transparent for AC field the first terms in series expansion of the susceptibility are (up to a shape dependent multiplication factor)

$$\mathrm{Re}\chi \approx -\left(R^2\mu\omega\sigma\right)^2 \tag{18}$$

$$\mathrm{Im}\chi \approx \left(R^2\mu\omega\sigma\right), \tag{19}$$

and $\mathrm{Re}\chi \ll \mathrm{Im}\chi$. A measurement of χ yields contactless estimation of the electrical conductivity σ.
In a linear or thermally activated flux flow state as the applied field approaches the upper critical field H_{c2}, the flux density in the superconductor $B \to \mu_0 H_{c2}$ and the flux flow resistivity ρ_f smoothly transforms to $\rho_n = 1/\sigma$

$$\frac{\rho_f}{\rho_n} \approx \frac{B}{\mu_0 H_{c2}} \tag{20}$$

as the phase transition between a mixed state and normal state is of second order (Bardeen Stephen model) (Bardeen, 1965). Flux flow resistivity may be estimated using Eq. 19.

3.5.2 Meissner state

At initial magnetization the superconductor is in Meissner state in field lower that H_{c1}. In this case the diffusivity is pure imaginary $D = i\omega\lambda^2$, where the flux penetration length is $\lambda = (\mu_0 n_s e^2/m)^{-1/2}$. The susceptibility of an infinitely long cylinder and slab in a parallel field, cylinder in a perpendicular field, and sphere is obtained like for normal state but replacing $(1+i)/\delta$ with i/λ (Brandt, 1998; Khoder & Couach, 1991; Lifshitz et al., 1984). The susceptibility as a function of $(\lambda/R)^2$ is shown in Fig. 2.
In a weak field, low temperature part of the susceptibility ($T/T_c < 0.5$) is proportional to the flux penetration length

$$\mathrm{Re}\chi(T) = -1 + a\lambda(T)/R. \tag{21}$$

A measurement of temperature dependence $\lambda(T)$ allows us to distinguish different pairing symmetries. While in conventional superconductors with an isotropic gap the quasiparticle excitations rise with increasing temperature as $\exp(-\Delta/k_B T)$, in nonconventional superconductors, for example HTS, a temperature dependence is power-law. As far as we know, it fails to fit experimental $\chi(T)$ at $T \to T_c$ even for well known $\lambda(T)$, at low temperatures.

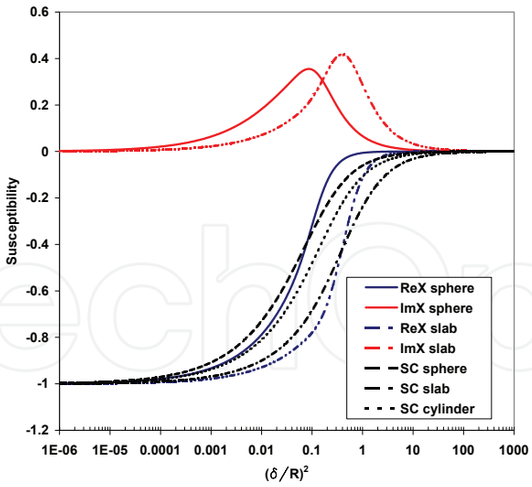

Fig. 2. The dependence of the complex AC susceptibility of a sphere and slab in a normal (ohmic) state in a parallel field on $(\delta/R)^2 \propto \rho_n$ and of the sphere, slab and cylinder in Meissner state on $(\lambda/R)^2 \propto 1/n_s$. In an ohmic state an absorption peak appears on Imχ, the height of which is characteristic of sample shape.

3.5.3 Bean critical state

The Bean model of the critical state is the case of a strong pinning when the flux density variation is quasi-static (frequency independent) in a slowly varying applied magnetic field and the flux density profile changes only when induced shielding current density reaches the critical depinning current density $j = \pm j_c$. An electric field is induced when the flux density changes. In a slab the flux density profile is linear $|\partial B_z(x)/\partial x| = \mu_0 j_c$ in flux penetrated regions and $|\mathbf{B}| = 0$ in untouched regions. The model assumes lower critical field $H_{c1} \to 0$, surface barrier $H_{barrier} \to 0$, and field independent critical depinning current density j_c, i.e. $j_c(B)$ is constant (Bean, 1964).

Analytical solutions for magnetization loops are known for an infinitely long slab or cylinder in a parallel field (Goldfarb, 1991) and thin disk (Clem & Sanchez, 1994; Mikheenko & Kuzovlev, 1993) or strip (Brandt, 1993) in a perpendicular field. In these cases the 3D partial differential equation (PDE) Eq. 13 reduces to a time independent 2D PDE due to sample shape symmetry.

The model to the disks was work out by Clem and Sanches who improved and corrected former model worked out by Mikheenko and Kuzovlev (Clem & Sanchez, 1994). The model is restricted to slow, quasistatic flux changes for which the magnitude of the electric field **E** induced by the moving magnetic flux is small in comparison with $\rho_f j_c$, where ρ_f is the flux flow resistivity. Under these conditions, the magnitude of the induced current density is close to the critical depinning current density. The validity of the model is restricted for $d \ll R$, $d \geq \lambda$ or if $d < \lambda$, that $\Lambda = 2\lambda^2/d \ll R$, where λ is the flux penetration length and Λ is the 2D screening length.

In the case of the infinitely long (or sufficiently long) sample (slab or cylinder) in parallel applied field the shielding current density is at a surface parallel with applied field,

$$\mu_0 j_\phi = -\partial B_z/\partial r \tag{22}$$

while in case of the sufficiently thin sample (disk or strip) in perpendicular applied field

$$\mu_0 j_\phi = \partial B_r / \partial z, \tag{23}$$

the shielding current appears simultaneously everywhere over the sample cross-section upon application of the field, and decreases everywhere simultaneously after a decrease of the field (Beek et al., 1996). The complete magnetic hysteresis loop can be obtained from the first magnetization curve, which is almost the same for the above cases. The hysteresis loop develops from the thin lens-shaped to parallelogram as the H_{ac} is increased or j_c decreases. The lens shape corresponds to partial penetration of the magnetic flux while the parallelogram occurs when the magnetization is saturated.
The component of the magnetization parallel to the applied periodically time varying field $H(\varphi) = H_{ac} \sin \varphi$ is

$$M_\mp = \mp \chi_0 H_{ac} \mathrm{S}\left(\frac{H_{ac}}{H_d}\right) \pm \chi_0 \left(H_{ac} \mp H\right) \mathrm{S}\left(\frac{H_{ac} \mp H}{2H_d}\right), \tag{24}$$

where M_- and M_+ are for decreasing and increasing applied field, respectively (Clem & Sanchez, 1994). A characteristic field $H_d = dj_c/2$, where d is the disk thickness and j_c is the critical depinning current density (temperature dependent). The function $\mathrm{S}(x)$ is defined as

$$\mathrm{S}\left(x\right) = \frac{1}{2x}\left[\arccos\left(\frac{1}{\cosh x}\right) + \frac{\sinh|x|}{\cosh^2 x}\right]. \tag{25}$$

3.5.4 Mapping of model susceptibility to experimental susceptibility

The model AC susceptibility is calculated for magnetization loops Eq. 24 using Eq. 11, i.e. in the same way as the experimental susceptibility (Youssef et al., 2009). To map the model susceptibility $\chi(H_{ac}/H_d)$ to the experimental temperature dependent susceptibility $\chi(T)$ we use a proportionality of the characteristic field to the critical depinning current density, $H_d = dj_c/2$, and a fact that experimentally observed temperature dependence, $j_c(T) = j_c(0)(1 - T/T_c)^n$, is power-law. Further, we need an inverse function for $j_c(T)$ and insert the amplitude of the applied field. Let us take

$$\frac{j_c(T)}{j_c(0)} = \frac{H_d(T)}{H_d(0)} = \left(1 - \left(\frac{T}{T_c}\right)^m\right)^n. \tag{26}$$

Relation between temperature T and ratio H_d/H_{ac}, i.e. experimental and model susceptibility, is obtained using inverse function for Eq. 26 and multiplying both the numerator and denominator, $H_d/H_d(0)$, by H_{ac}

$$\left(\frac{T}{T_c}\right)_{model} = \left(1 - \left(\frac{H_{ac}}{H_d(0)}\frac{H_d}{H_{ac}}\right)^{1/n}\right)^{1/m}. \tag{27}$$

We have four free parameters $c \equiv H_{ac}/H_d(0)$, n, m, and T_c to match the model and experimental susceptibility

$$\left[\left(1 - \left(c\frac{H_d}{H_{ac}}\right)^{\frac{1}{n}}\right)^{\frac{1}{m}}, \chi\left(\frac{H_d}{H_{ac}}\right)\right] \longleftrightarrow \left[\frac{T}{T_c}, \chi(T)\right]. \tag{28}$$

When we find c, n, m, and T_c, the zero temperature critical depinning current density is

$$j_c(0) = 2H_{ac}/cd \tag{29}$$

and its temperature dependence is given by Eq. 26.

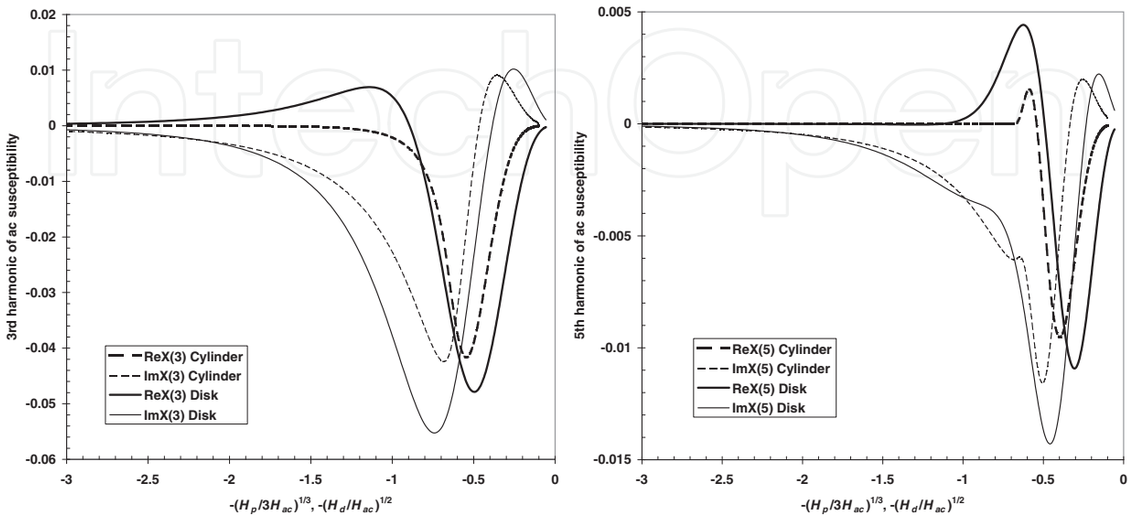

(a) The third harmonic of the AC susceptibility. (b) The fifth harmonic of the AC susceptibility.

Fig. 3. Differences in the harmonics of AC susceptibility for models of cylinders and disks. The susceptibility is plotted versus "model temperature" given by Eq. 27 (Youssef et al., 2009). Here H_p is the characteristic field for a cylinder, $H_p = Rj_c$.

3.5.5 Interpretation of complex AC susceptibility

The real part of the fundamental AC susceptibility represents a magnetic energy of the sample stored in the diamagnetic shielding current. The imaginary part of the fundamental susceptibility is related to losses caused by resistive response (dissipation).

In normal state or in flux flow state the AC susceptibility is a function of applied field frequency, conductivity (resistivity), and temperature but is independent of the field amplitude. On the other hand, in a case of strong pinning the AC susceptibility is a function of the applied field amplitude, critical depinning current density, and temperature but is independent of frequency. Nonlinear dependence of the sample magnetization on applied field amplitude generates harmonics of AC susceptibility. Their behavior is characteristic for a given sample shape. Due to a symmetry of the magnetization loops, $M(H) = -M(-H)$, the coefficients of even harmonics of the AC susceptibility are zero.

4. Experimental results on critical state in type II superconductors

Recently developed second generation of the high temperature superconductor wires on the basis of YBaCuO films and Nb films for superconductor electronics production represent proper materials to study models to the critical state in hard superconductors.

4.1 Materials

The Nb film of thickness of 250 nm was deposited by a dc magnetron sputtering in Ar gas on 400 nm thick silicon-dioxide buffer layer which was grown by a thermal oxidation of a silicon single crystal wafer (May, 1984). The film is polycrystalline with texture of a preferred orientation in the (110) direction and is highly tensile. Grain size is about 100 nm. The square samples of 5×5 mm^2 in dimensions were cut out from the 3-inch wafer.
Second-generation high temperature superconductor wire (2G HTS wire) consists of a 50 μm nonmagnetic nickel alloy substrate (Hastelloy), 0.2 μm of a textured MgO-based buffer stack deposited by an assisting ion beam, 1 μm RE-$Ba_2Cu_3O_x$ superconducting layer SmYBaCuO deposited by metallo-organic chemical vapor deposition, and 2 μm of Ag, with 40 μm total thickness of surround copper stabilizer (20 μm each side) .[9] The sample is cut into 4 mm long segment of 4 mm wide wire.

4.2 Estimation of the critical depinning current density and its temperature dependence

Since the model susceptibility is not given analytically the standard fitting procedures cannot be applied here. A convenient way to map the model susceptibility to the experimental one is to plot the experimental susceptibility as a function of reduced temperature T/T_c and superimpose the model susceptibility by fitting parameters c, n, and m in Eq. 27 and T_c interactively (manually), see Fig. 4. The critical depinning current density estimated using Eq. 29 is $j_c(0) = 3 \times 10^{11}$ A/m^2 in the Nb film with temperature dependence $j_c(T) = j_c(0)[1 - (T/T_c)]^{3/2}$. The critical depinning current density found in the YBCO wire is $j_c(0) = 10^{12}$ A/m^2 with steeper temperature dependence, $j_c(T) = j_c(0)[1 - (T/T_c)]^2$. This result well agrees with j_c estimated using a four point probe contact measurements (Youssef et al., 2009; 2010).

5. Conclusion

The thin film type II superconductors with a strong pinning allowed us to verify the complete analytical model of a response of a thin disk in the Bean critical state to an applied time varying magnetic field. On the other hand, the application of this model gives a contactless estimation of the critical depinning current density and its temperature dependence.
To observe the characteristic critical state response from an YBCO sample as is shown in Fig. 4 at lower temperatures the applied time varying field has to be of the order of 0.1 T at 77 K and of the order of 1 T at 4.2 K. Such fields may rather be generated using a normal (nonsuperconducting) solenoid that avoids a residual field of flux lines trapped in the superconducting solenoid winding and guaranties a linear $H(I)$ relation. However, dissipated power will be large. Also, since the induced magnetic moment will be large, there is no need for a sensitive superconducting detection system, but a detector with high linearity and flat frequency and phase response is necessary as the maximum amplitude of 3rd harmonic is only 6% and 5th harmonic of only 1% of the real part of the fundamental susceptibility.
The fit to the model reveals an excess of few % of the real part of the susceptibility as temperature decreases to zero. This diamagnetic contribution is due to the temperature

[9] Wire type SCS4050 SuperPower, Inc., Schenectady, NY 12304 USA. The critical current of the wire as estimated using four probe method and 1 μV/cm criterion is from 80 to 110 A at 77 K (97 A for our piece of wire).

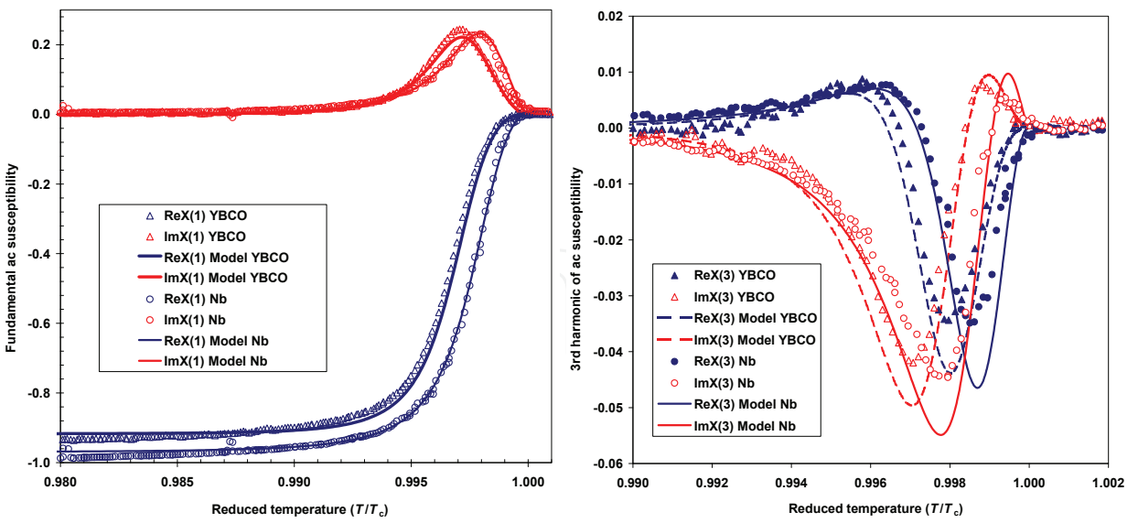

(a) The fundamental AC susceptibility. (b) The third harmonic of the AC susceptibility.

Fig. 4. Temperature dependence of the AC susceptibility of Nb and YBCO films in perpendicular field $\mu_0 H_{ac} = 10$ μT and $f = 1.5625$ Hz (Youssef et al., 2010).

dependent flux penetration length $\lambda(T)$ which depends exponentially on temperature in conventional superconductors (Nb) and obeys a power-law in unconventional ones (YBCO). As was shown by Brandt, the normalized magnetization curves for hard (Bean) superconductors obtained by a numerical treatment differ very little for similar geometries (Brandt, 1996): between strips and circular disks the relative difference is < 0.011, between thin circular and quadratic disks the difference is < 0.002. This makes an application of fully analytical models for contactless estimation of the critical depinning current density and its temperature dependence favorable.

6. Acknowledgements

The authors are grateful to SuperPower, Inc. for providing us with 2G HTS YBCO wire, and to F. Soukup and R. Tichy for technical assistance. This work was supported by Institutional Research Plan AVOZ10100520, Research Project MSM 0021620834 (Ministry of Education, Youth and Sports of the Czech Republic), the Czech Science Foundation under contract No. 202/08/0722, (Javorsky SVV grant 2011-263303) and ESF program NES.

7. References

Anderson, P.W. (1962). Theory of flux creep in hard superconductors, *Phys. Rev. Lett.* Vol. 9:309-311.

Anderson, P.W. & Kim, Y.B. (1962). Hard Superconductivity: Theory of the Motion of Abrikosov Flux Lines, *Rev. Mod. Phys.* Vol. 36:39-43.

Bardeen, J. (1962). Critical fields and currents in superconductors, *Rev. Mod. Phys.* Vol. 34:667-681.

Bean, C.P. (1964). Magnetization of High-Field Superconductors, *Rev. Mod. Phys.* Vol. 36:31-39.

van der Beek, C.J., Indenbom, M.V., D'Anna, G., Benoit, W. (1996). Nonlinear AC susceptibility, surface and bulk shielding, *Physica C* Vol. 258:105-120.

Blatter, G., et al. (1994) Vortices in high-temperature superconductors, *Phys. Mod. Phys.* Vol. 66:1125-1388.

Brandt, E.H., et al. (1993). Type-II Superconducting Strip in Perpendicular Magnetic Field, *Europhys. Lett.* Vol. 22, No. 9: 735 - 740

Brandt, E.H. (1996). Superconductors of finite thickness in a perpendicular magnetic field: Strips and slabs, *Phys. Rev. B* Vol. 54: 4246-4264.

Brandt, E.H. (1998). Superconductor disks and cylinders in an axial magnetic field. I. Flux penetration and magnetization curves, *Phys. Rev. B* Vol. 58: 6506-6522; Superconductor disks and cylinders in an axial magnetic field: II. Nonlinear and linear ac susceptibilities, *Phys. Rev. B* Vol. 58: 6523-6533

Chen, D.-X., et al. (2007). Field dependent alternating current susceptibility of metalorganically deposited YBa2Cu3O7-d films, *J. Appl. Phys.* 101: 073905-.

Clem, J.R. & Sanchez, A. (1994). Hysteretic ac losses and susceptibility of thin superconducting disks, *Phys. Rev. B* Vol. 50: 9355-9362.

deGennes, P. G. (1966), In: *Superconductivity of Metals and alloys* (Benjamin, New York, 1966).

Goldfarb, R.B., Lelenthal, M., Thompson, C.A., Alternating-field susceptometry and magnetic susceptibility of superconductors, In: *Magnetic Susceptibility of Superconductors and Other Spin Systems*, edited by R. A. Hein (Plenum Press 1991), p. 49.

Gömöry, F. (1997). Characterization of high-temperature superconductors by AC susceptibility measurements, *Supercond. Sci. Technol.* Vol. 10: 523-542.

Koshelev A.E., Vinokur V.M. (1994), Dynamic meltig of the vortex lattice, *Phys. Rev. Lett.* Vol. 73: 3580-3583.

Khoder, A.F. and Couach, M. (1991). Early theories of χ' and χ'' of superconductors; the controversial aspects, In: *Magnetic Susceptibility of Superconductors and other Spin Systems*, New York and London: Plenum Press. p 213-228.

Lifshitz, E.M. et al. (1984) In: *Electrodynamics of Continuous Media*, Vol. 8 (Course of Theoretical Physics), Ed. Butterworth-Heinemann.

May T. (1984), Ph.D. Thesis, Institute for Physical High Technology, Jena, Germany 1999.

Mikheenko P. N. & Kuzovlev Yu. E. (1993), Inductance measurements of HTSC films with high critical currents, *Physica C* Vol. 204:229-236.

Press, W.H., et al. (1992). In: *Numerical Recepies in C*, Cambridge University Press, ISBN 0 521 43720 2, Cambridge. p 496 - 536.

Pearl, J. (1964). Current distribution in superconducting films carrying quantized fluxoids, *Appl. Phys. Lett.* 5:65-66.

Sanchez, A. & Navau, C. (1999). X, *IEEE Trans. Appl. Supercond.* Vol. 9:2195-

Tinkham, M. (1996) In: *Introduction to Superconductivity*, (McGraw-Hill, New York, 1996).

Tsoy, G.M. et al. (2000). High-resolution SQUID magnetometer, *Physica B*, Vol. 284, Part 2:2122-2123.

Vrba, J. & Robinson, S.E. (2001). Signal processing in magnetoencephalography. *Methods*, Vol. 25:249-271.

Wellstood, F.C., et al. (1987) Low-frequency noise in dc superconducting quantum interference devices below 1 K *Appl. Phys. Lett.* 50:772-774.

Youssef, A., Svindrych, Z., Janu, Z. (2009) Analysis of magnetic response of critical state in second-generation high temperature superconductor YBa2Cu3Ox wire, *J. Appl. Phys.* Vol. 106: 063901-1-1063901-6.

Youssef, A., et al. (2010). Contactless Estimation of Critical Current Density and Its Temperature Dependence Using Magnetic Measurements, *Acta Physica Polonica A* Vol. 118, No. 5:1036-1037.

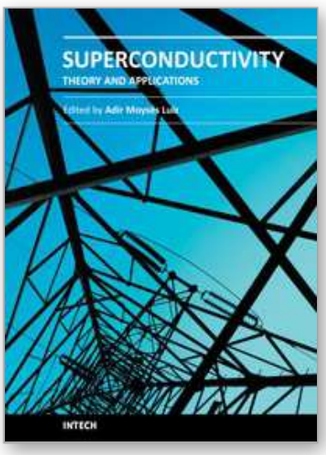

Superconductivity - Theory and Applications

Edited by Dr. Adir Luiz

ISBN 978-953-307-151-0
Hard cover, 346 pages
Publisher InTech
Published online 18, July, 2011
Published in print edition July, 2011

Superconductivity was discovered in 1911 by Kamerlingh Onnes. Since the discovery of an oxide superconductor with critical temperature (Tc) approximately equal to 35 K (by Bednorz and Müller 1986), there are a great number of laboratories all over the world involved in research of superconductors with high Tc values, the so-called â€œHigh-Tc superconductorsâ€. This book contains 15 chapters reporting about interesting research about theoretical and experimental aspects of superconductivity. You will find here a great number of works about theories and properties of High-Tc superconductors (materials with Tc > 30 K). In a few chapters there are also discussions concerning low-Tc superconductors (Tc < 30 K). This book will certainly encourage further experimental and theoretical research in new theories and new superconducting materials.

How to reference

In order to correctly reference this scholarly work, feel free to copy and paste the following:

Janu, Zdeněk Švindrych, Ahmed Youssef and Lucia Baničová (2011). Critical state analysis using continuous reading SQUID magnetometer, Superconductivity - Theory and Applications, Dr. Adir Luiz (Ed.), ISBN: 978-953-307-151-0, InTech, Available from: http://www.intechopen.com/books/superconductivity-theory-and-applications/critical-state-analysis-using-continuous-reading-squid-magnetometer

INTECH
open science | open minds

InTech Europe
University Campus STeP Ri
Slavka Krautzeka 83/A
51000 Rijeka, Croatia
Phone: +385 (51) 770 447
Fax: +385 (51) 686 166
www.intechopen.com

InTech China
Unit 405, Office Block, Hotel Equatorial Shanghai
No.65, Yan An Road (West), Shanghai, 200040, China
中国上海市延安西路65号上海国际贵都大饭店办公楼405单元
Phone: +86-21-62489820
Fax: +86-21-62489821

IntechOpen